Analysis of the combined and single effects of LULC and climate change on the streamflow of the Upper Blue Nile River Basin Using statistical trend tests, remote sensing landcover maps and the SWAT model

5   Dagnenet F. Mekonnen[1, 2], Zheng Duan[1], Tom Rientjes[3], Markus Disse[1]

[1]Chair of Hydrology and River Basin Management, Faculty of Civil, Geo and Environmental Engineering, Technische Universität München, Arcisstrasse 21, 80333, Munich, Germany.
[2]Amhara Regional State Water, Irrigation and Energy Development Bureau, Bahirdar, Ethiopia
[3]Department of Water Resources, Faculty of Geo-Information Science and Earth Observation (ITC), University of Twente,
10 Enschede, Netherlands
Correspondence to: Dagnenet F. (dagnfenta@yahoo.com)

Abstract: Understanding the response of land use/land cover (LULC) and climate change has become a priority issue for water management and water resource utilization of the Nile basin. This study assesses the long-term trends of rainfall and
15 streamflow to analyse the response of LULC and climate changes on the hydrology of the study area. The MK test showed statistically insignificant increasing trends for annual, monthly and long rainy season rainfall series while no trend for daily, short rainy and dry season rainfall series. However, the Pettitt test could not detect any jump point in basin wide rainfall series except for daily rainfall time series. In contrast, the result of MK-test for daily, monthly, annual and seasonal (long and short rainy season and dry season) time series streamflow showed a positive trend and the trend magnitude is statistically
20 significant. Landsat satellite images for 1973, 1985, 1995 and 2010 were used for LULC change detection analysis. The LULC change detection findings indicate that expansion of cultivated land and the reduction of forest coverage were significant before the period 1995. After 1995, the forest coverage began to increase while the cultivated land getting reduced. Statistically, forest coverage changed from 17.4 % to 14.4 %, 12.2 % and 15.6 % while cultivated land changed from 62.9 % to 65.6 %, 67.5 % and 63.9 % from 1973 to 1985, 1995 and 2010 respectively.

The hydrological model result showed that mean annual streamflow increased by 16.9 % between the 1970s and the 2000s due to the combined effect of LULC and climate change. The single effect of LULC change on streamflow analysis suggested that LULC change affects surface run-off and base flow. This could be attributed to the 5.1 % reduction in forest coverage and 4.6 % increase in cultivated land. Effects of climate change revealed that the increased rainfall intensity and
30 number of extreme rainfall events from 1971 to 2010 have significantly affected the surface run-off and base flow. The single impacts of climate change is significant as compared to the impacts of LULC change for the hydrology of UBNRB.

1. Introduction

The Abay (Upper Blue Nile) River in Ethiopia contributes more than 60 % of the water resources of the Nile river (McCartney et al., 2012). Hence, the Ethiopian government has carried out a series of studies to tap this huge potential water resource aiming to significantly increase large reservoir for water storage in the Upper Blue Nile River Basin (UBNRB) both
5   for irrigation and hydropower development, in order to support national development and to reduce poverty (BCEOM, 1998). As a result, large scale irrigation and hydropower projects has been planned and realized along the main stem of Blue Nile river such as Grand Ethiopian Renaissance Dam (GERD), the largest dam in Africa when it is completed. However, its hydrology is influenced by high variations in climate and altitude/topography, land use/cover (LULC) change exhibiting highly seasonal flows. Therefore, effective planning, management and regulation of water resource developments is required
10 to prevent conflict between competing water users particularly downstream countries such as Sudan and Egypt. Conflict can be reduced and benefits maximized if careful management of water resource is established.

This can be achieved only by understanding the hydrological processes and sources impacting water quantity such as
15 LULC and climate change as they are the key driving forces that can modify the hydrology and water availability of the watershed (Oki and Kanae, 2006; Woldesenbet *et al.*, 2017b; Yin *et al.*, 2017a). LULC can modify the rainfall path into run-off by altering critical water balance components, such as surface run-off, groundwater recharge, infiltration, interception and evaporation (Marhaento et al., 2017; Woldesenbet et al., 2017b). The UBNRB already experiences significant spatial and temporal climate variability (McCartney et al. 2012), less than 500 mm yr^{-1} of precipitation falls near the Sudan border
20 to more than 2,000 mm yr^{-1} in some places in the southern basin (Awulachew et al., 2009). Potential evapotranspiration (ET) also varies considerably and is highly correlated with altitude, it exceeds 2,200 mm yr^{-1} near the Sudan border from approximately 1,300 to 1,700 mm yr^{-1} in the Ethiopian highlands (McCartney et al., 2012). As a result of the precipitation and ET cycles, stream flow is highly characterized by extreme seasonal and inter-annual variability.

25 A literature review shows that there are few sub-basin and basin level studies carried out in the UBNRB, with most studies focusing on trend analysis of precipitation and streamflow Considering precipitation, most studies e.g.,(Bewket and Sterk, 2005; Cheung et al., 2008; Conway, 2000; Gebremicael et al., 2013; Melesse et al., 2009; Rientjes et al., 2011; Seleshi and Zanke, 2004; Teferi et al., 2013; Tekleab et al., 2014; Tesemma et al., 2010) reported no significant trend in annual and seasonal precipitation totals within the Lake Tana sub-basin, While Mengistu et al. (2014) reported statistically non-
30 significant increasing trends at annual and seasonal rainfall series except a short rainy season (Belg) from February to May.

For the streamflow of the UBNRB, (Gebremicael et al., 2013) reported statistically significant increasing long-term mean annual streamflow at the El Diem gauging station. However, (Tesemma et al., 2010) reported no statistically significant trend for the long-term annual streamflow at ElDiem gauging station, but a significantly increasing trend at Bahirdar and

Kessie stations. At the sub-basin scale, Rientjes et al. (2011) reported a decreasing trend for the low streamflows of Gilgel Abay sub-basin (Lake Tana catchment, the Blue Nile head waters) during the period (1973–2005), specifically by 18.1 % and 66.6 % in the periods 1982–2000 and 2001–2005, respectively. However, for the same periods, the high streamflows show an increase by 7.6 % and 46.6 % due to LULC change and seasonal variability of rainfall.

Although, substantial progress has been made in assessing the impacts of LULC and climate change on the hydrology of the UBNRB, only few studies have attempted to assess the attribution of changes in the water balance to LULC and climate change. Woldesenbet et al. (2017b), used an integrated approach comprising SWAT hydrological modeling and partial least squares regression (PLSR) to quantify the contributions of changes in individual LULC classes to changes in hydrological components in two watersheds namely: Lake Tana and Beles sub basins. (Woldesenbet et al., 2017b) reported that expansion of cultivation land and decline in woody shrub/woodland appear to be major environmental stressors affecting local water resources such as increasing surface run-off and decreasing of ground water in both watersheds but the impacts of climate change is missing. However, proper water resource management requires an in-depth understanding on the aggregated and disaggregated effects of LULC and climate changes on streamflow and water balance components as the interaction between LULC, the climate characteristics and the underlying hydrological processes are complex and dyanmic (Yin *et al.*, 2017a). .

Therefore, the objectives of this study are as follows (i) assess the long-term trend of rainfall and streamflow (ii) analyse the LULC change (iii) examining the streamflow responses to combined and isolated effects of LULC and climate changes in the UBNRB. This can be done using a combined analysis of statistical trend test, change detection of LULC derived from satellite remote sensing and hydrological modelling during the period 1971-2010.

2. Study area

The UBNRB is located in the northwest of Ethiopia with an approximate catchment area of 172,760 km^2. Topography of the basin is typically characterized by highlands, hills, valleys and occasional rock peaks with elevations that range from 500 m.a.s.l to above 4000 m.a.s.l (Figure 1). According to BCEOM (1998), the larger portion of the basin (2/3) lies in the highlands of Ethiopia with annual rainfall ranging from 800 mm to 2,200 mm. A central and south-eastern area is characterised by relatively high rainfall (1400-2200 mm) and less than 1200 mm rainfall occurred in most of the eastern and north-west parts of the basin. Mekonnen and Disse (2018) showed that the UBNRB has a mean areal annual rainfall of 1452 mm, and a mean annual minimum and maximum temperature of 11.4 ^{o}C and 24.7 ^{o}C respectively.

The climate of the study area is characterized by tropical climate and dominated by its high altitude. The climate is also governed by the movement of the Inter-Tropical Convergent Zone (ITCZ) (Conway, 2000; Mohamed et al., 2005). NMA (2013) classified the climate into three seasons in Ethiopia. The main rainy season (Kiremt) lasts generally from June to

September during which south-west winds bring rains from the Atlantic Ocean. About 70-90 % of total rainfall occurs during this season. A dry season (Bega) lasts from October to January and the short rainy season (Belg) lasts from February to May. According to BCEOM (1998), the average annual discharge is estimated about 49.4 Billion Cubic Meter (BCM), with the low flow month (April) equivalent to less than 2.5 % of that of the high flow month (August), at the Ethio-Sudan border (El Diem). The analysis of this study revealed that the long-term (1971-2010) mean annual volume of flow at El Diem is 50.7 BCM, with the low flow (dry season) contributing 21.1 % and the short rainy season accounting for about 6.2 %, while most flow occurred during the rainy season, contributing about 73 % (Table 1). The land cover of the basin essentially follows the divide between highland and lowland. The highlands are predominantly covered by farmlands (about 90 %), bush and shrubs. The lowlands, in contrast, are still largely untouched by development, as a result, woodlands, bush and shrub lands are the dominant forms of land cover (BCEOM, 1998).

3. Input data sources

In this study, non-parametric Mann-Kendal (MK) (Kendall, 1975; Mann, 1945) statistics and Soil and Water Assessment Tool (SWAT) developed by the Agricultural Research Service of the United States Department of Agriculture (USDA-ARS) (Arnold et al., 1998) are used for statistical trend analysis and water balance modelling respectively. Details about the methods are described under section 4. The input datasets used for SWAT model can be categorised into weather and streamflow data and spatially distributed datasets.

3.1 Weather and streamflow data

The daily weather variables used in this study for trend analysis and for driving water balance model are precipitation, minimum temperature (Tmin), maximum air temperature (Tmax), relative humidity (RH), hours of sunshine (SH) and wind speed (WS). These weather data were obtained from the Ethiopian National Meteorological Agency (ENMA) for the period 1971-2010. The daily streamflow data for over 25 gauging stations was collected from the Federal Ministry of Water Irrigation and Electricity of Ethiopia for the period 1971-2010. After intensive and rigorous analyses of weather data, considerable time series data were missed in most stations (see Table s01) due to civil war, defected and outdated devices. As a result, the available data constrained us to focus only for 15 stations (Figure 1) in which rainfall data are relatively more complete. All 15 stations were used for trend analysis while the 10 stations which have complete climate variables such as Tmax, Tmin, RH, WS and SH were used as input for SWAT model Figure 1.

We have used spatial interpolation such as the inverse distance weighting method (IDWM) and linear regression techniques (LR) to fill the gaps. Similar approaches or methods were applied by Uhlenbrook et al. (2010) for the Gilgel Abbay sub-basin, which is the head water of UBNRB. The selection and number of adjacent stations are critically important for the accuracy of the estimated results. As mentioned by Woldesenbet et al. (2017a), different authors used different criteria to

select neighboring stations. Because of low station density of the study area, for most stations, a geographic distance of 100 km were considered to select neighbouring stations. If no station is located within 100 km of the target station, the search distance is increased until the minimum of one suitable station is reached. After the neighbouring stations were selected, the two methods (IDWM and LR) were tested to fill in missing datasets. The performance of the candidate approaches was

5   evaluated using the statistical metrics such as root mean square error (RMSE), mean absolute error (MAE), correlation coefficient (R^2) and percent bias (% bias) between observed and estimated values for the target stations. Equally weighted statistical metrics is applied to compare the performance of selected approaches at target stations to establish ranking. A score was assigned to each candidate approach according to the individual metrics; e.g. the one achieving the smallest RMSE and MAE, or % bias has got score 1, and so on. The final score is obtained by summing up the score pertained to each

10 candidate approaches at each stations. The best method is the one having the smallest score. The monthly, seasonal and annual weather data were aggregated from the daily time series data after filling the gaps. While filling the missing data uncertainty is expected due to the low station density, poor coorelations and considerable missing records. Similar techniques and approaches were used for the analysis and filling the missed records of streamflow data.

3.2 Spatial Data:

15 Required spatially distributed data for SWAT model includes tabular and spatial soil data, tabular and spatial land use /cover information, and elevation data. A Shuttle Radar Topographic Mission Digital Elevation Model (SRTM DEM) of 90 metres resolution from the Consultative Group on International Agricultural Research-Consortium for Spatial Information (CGIAR-CSI; http://srtm.csi.cgiar.org/SELECTION/inputCoord.asp) was used to delineate the watershed and to analyse the drainage patterns of the land surface terrain. Subbasin parameters such as slope gradient, slope length of the terrain, and the stream

20 network characteristics such as channel slope, length, and width were derived from the DEM.

The soil map developed by the Food and Agriculture Organization of the United Nations (FAO-UNESCO) at a scale of 1:5,000,000 downloaded from (http://www.fao.org/soils-portal/soil-survey/soil-maps-and-databases/faounesco-soil-map-ofthe-world/en/) was used for SWAT model. The soil information such as soil textural and physiochemical properties needed

25 for the SWAT model was extracted from Harmonized World Soil Database v1.2, a database that combines existing regional and national soil information (http://www.fao.org/soils-portal/soil-survey/soil-maps-and-databases/harmonized-world-soil-databasev12/en/) in combination with information provided by FAO-UNESCO soil map (Polanco et al., 2017).

The LULC maps, representing one of the most important driving factors to affect surface run-off and evapo-transpiration in a

30 basin were produced from satellite remote sensing Landsat images for 1973, 1985, 1995 and 2010 at a scale of 30x30 m resolution. Detail image processing and classification approaches is described under section 4.2.

4. Methodology

4.1 Trend Analysis

The non-parametric Mann-Kendal (MK) (Kendall, 1975; Mann, 1945) statistics is chosen to detect trends for precipitation and streamflow time series data as it is widely used for effective water resource planning, design and management (Yue and Wang, 2004). Its advantage over the parametric tests, such as t-test, is that the MK test is more suitable for non-normally distributed, andmissing data, which are frequently encountered in hydrological time series (Yue *et al.*, 2004). However, the existence of positive serial correlation in a time series data affects the result of MK test. If serial correlation exists in a time series data, the MK test rejects the null hypothesis of no trend detection more often than specified by the significance level (von Storch, 1995).

In order to limit the influence of serial correlation on the MK test, pre-whitening was proposed by von Storch (1995). And also, the Effective or Equivalent Sample Size (ESS) method developed by Hamed and Rao (1998) has been proposed to modify the variance. However, the study by (Yue et al., 2002) reported that von Stroch's pre-whitening is effective only when no trend exists and the rejection rate of the ESS approach after modifying the variance is much higher than the actual (Yue et al., 2004). Then, Yue et al. (2002) proposed trend-free pre-whitening (TFPW) prior to applying the MK trend test in order to minimize it's limitation. This study therefore employed TFPW to remove the serial correlation and to detect a trend in a time data series with significant serial correlation. Further details can be found in (Yue et al., 2002). All the trend results in this paper have been evaluated at the 5 % level of significance to ensure an effective exploration of the trend characteristics within the study area.

Change point test

The Pettitt test is used to identify if there is a point change or jump in the data series (Pettitt, 1979). This method detects one unknown change point by considering a sequence of random variables X 1, X 2, …, XT that may have a change point at N if Xt for t = 1, 2, …, N has a common distribution function F1(x) and Xt for t = N + 1, …, T has a common distribution function F2(x), and F1(x) ≠ F 2(x).

Sen's slope estimator

The trend magnitude is estimated using a non-parametric median based slope estimator proposed by (Sen, 1968) as it is not greatly affected by gross data errors or outliers, and it can be computed when data are missing. The slope estimation is given by:

$$\beta = \text{Median} \left[\frac{X_j - X_k}{j - k} \right] \quad \text{for all } k < j, \quad \text{............1}$$

Where $1 < k < j < n$, and β is considered as median of all possible combinations of pairs for the whole data set. A positive value of β indicates an upward (increasing) trend and a negative value indicates a downward (decreasing) trend in the time series. All MK trend test, Pettitt change point detection and sen's slope analyses were conducted using the XLSTAT add-ins tool from excel (www.xlstat.com).

4.2 Remote sensing land use/cover map

4.2.1. Landsat image acquisition

Landsat images of the year 1973, 1985, 1995 and 2010 were accessed free-of-charge from the US Geological Survey (USGS) Center for Earth Resources Observation and Science (EROS) via http://glovis.usgs.gov. The Landsat image scenes were selected based on the criteria of acquisition period, availability and percentage of cloud cover. According to the recommendation of (Hayes and Sader, 2001), images needed to be acquired for the same acquisition period, in order to reduce scene-to-scene variation due to sun angle, soil moisture, atmospheric condition and vegetation phenology differences. Hence, cloud free images were collected for the dry months of January to May. However, as the basin covers large area, each period of LULC map comprised of 16 Landsat scenes, therefore, it was difficult to access all the scenes in a dry season of a single year. Hence, images were acquired ±1 year for each time period and also some images were acquired in the month of November and December. For 1973, for example, 16 Landsat MSS image scenes were acquired (10 images in the month of January, 4 images in the month of December and 2 images in the month of November) in1973 (±1 years) and merged to arrive at one LULC representation for selected years. Please see supplement Table s02for the detail of landsat images.

4.2.2 Pre-processing and processing images

Several standard pre-processing methods including geometric and radiometric correction were implemented to prepare the LULC maps from Landsat images. Even though there are many different classification methods, supervised and unsupervised classifications are the two widely used methods for landcover classification from remote sensing images. Hence, in this study, a hybrid supervised/unsupervised classification approach was carried out to classify the images of 2010 (LandsatTM). Firstly, Iterative Self-Organizing Data Analysis (ISODATA) clustering was performed to determine the spectral classes or land cover classes of the image. Secondly, polygons for all of the training samples based on the identified LC classes were digitized using ground truth data and then the samples for each land cover type were aggregated. Finally, a supervised classification was performed using a maximum likelihood algorithm in order to extract four LULC classes.

A total of 488 Ground Control Points (GCPs) regarding landcover types and their spatial locations were collected from field observation in March and April, 2017 using a Global Positioning System (GPS). Reference data (GCPs) were collected and taken from areas where there had not been any significant landcover change between 2017 and 2010 by interviewing local

elderly people, supplemented by using high resolution Google Earth Images and priori-knowledge of the first author. As many as 288 points were used for accuracy assessment and 200 points were used for developing training sites to generate a signature for each land cover type. The accuracy of the classifications was assessed by computing the error matrix (also known as confusion matrix) that compares the classification result with ground truth information as suggested by DeFries and Chan (2000). A confusion matrix lists the values for known cover types of the reference data in the columns and for the classified data in the rows (Banko, 1998) as shown in Table 5. From the confusion matrix, Another discrete multivariate technique of use in accuracy assessment is called KAPPA (Congalton, 1991). The statistical metrics for KAPPA analysis is a Kappa coefficient, which is another measure of the proportion of agreement or accuracy. The Kappa coefficient is computed as

$$\mathrm{K} = \frac{N \sum_{i=1}^{i=r} x_{ii} \sum_{i=1}^{r}(x_{i+}*x_{+i})}{N^2 - \sum_{i=1}^{r}(x_{i+}*x_{+i})} \dots\dots\dots\dots\dots\dots\dots\dots\dots\dots\dots\dots \text{ 2}$$

where r is the number of rows in the matrix, xii is the number of observations in row i and column i, x i+ and x +i are the marginal totals of row i and column i, respectively, and N is the total number of observations.

Once the landcover classification of the year 2010 Landsat image is completed and its accuracy is checked, the NDVI differencing technique (Mancino *et al.*, 2014) was applied to classify the images of 1973, 1985 and 1995. This technique was chosen to increase the accuracy of classification as it is hard to find an accurately classified digital or analogue LULC map of the study area during the period of 1973, 1985 and 1995. And also, the information obtained from the elders are more subjective and its reliability is questionable when there is considerable time gap. We first calculated the NDVI from the Landsat MSS (1973) and three pre-processed Landsat TM images (1985, 1995, 2010) following the general normalized difference between band TM4 and band TM3 images eqn. 3. The resulting successive NDVI images were subtracted each other to assess the ΔNDVI image with positive (vegetation increase), negative (vegetation cleared) and no change on a 30 x 30 m pixel resolution (eqn.4-6). The Landsat MSS 60m x 60m pixel size data sets were resampled to a 30 m x 30 m pixel size using the 'nearest neighbour' technique in order to have similar pixel sizes for the different images without altering the original pixel values of the image data.

$$\mathrm{NDVI} = \frac{(TM4-TM3)}{(TM4+TM3)} \text{ or } \frac{(MSS_3-MSS_2)}{(MSS_3+MSS_2)} \qquad\qquad (3)$$

$$\mathrm{\Delta NDVI}_{1995/2010} = \mathrm{NDVI}_{1995} - \mathrm{NDVI}_{2010} \qquad\qquad (4)$$

$$\mathrm{\Delta NDVI}_{1985/1995} = \mathrm{NDVI}_{1985} - \mathrm{NDVI}_{1995} \qquad\qquad (5)$$

$$\mathrm{\Delta NDVI}_{1973/1985} = \mathrm{NDVI}_{1973} - \mathrm{NDVI}_{1985} \qquad\qquad (6)$$

The ΔNDVI image was then reclassified using a threshold value calculated as μ ± n*σ; where μ represents the ΔNDVI pixels value mean, and σ the standard deviation. The threshold identifies three ranges in the normal distribution: (a) the left tail (ΔNDVI < μ - n*σ); (b) the right tail (ΔNDVI > μ + n*σ); and (c) the central region of the normal distribution (μ - n*σ < ΔNDVI < μ + n*σ). Pixels within the two tails of the distribution are characterized by significant landcover changes, while pixels in the central region represent no change. To be more conservative n=1 was selected for this study to narrow the ranges of the threshold for reliable classification. The standard deviation (σ) is one of the most widely applied threshold identification approaches for different natural environments based on different remotely sensed imagery (Hu *et al.*, 2004; Jensen, 1996; Lu *et al.*, 2004; Mancino *et al.*, 2014; Singh, 1989) as cited by Mancino *et al.* (2014).

ΔNDVI pixel values (2010-1995) in the central region of the normal distribution (μ - n·σ < ΔNDVI < μ + n·σ) represent an absence of landcover change between two different periods (i.e. 1995 and 2010), therefore, pixels of 1995 corresponding to no landcover change can be classified as similar to the 2010 landcover classes. Pixels with significant NDVI change are again classified using supervised classification, taking signatures from the already classified no change pixels. Likewise, landcover classification of 1985 and 1973 images was performed based on the classified images of 1995 and 1985 respectively. Finally, after classifying the raw images of Landsat into different landcover classes, change detection which requires the comparison of independently produced classified images (Singb, 1989) was performed by the post-classification method. The post-classification change detection comparison was conducted to determine changes in LULC between two independently classified maps from images of two different dates. Although this technique has some limitations, it is the most common approach as it does not require data normalization between two dates (Singh, 1989) because data from two dates are separately classified, thereby minimizing the problem of normalizing for atmospheric and sensor differences between two dates.

4.3 SWAT hydrological model

The Soil and Water Assessment Tool (SWAT) is an open-source-code, semi-distributed model with a large and growing number of model applications in a variety of studies ranging from catchment to continental scales (Allen *et al.*, 1998; Arnold *et al.*, 2012; Neitsch *et al.*, 2002). It enables to evaluates the impact of LULC and climate change on water resources in a basin with varying soil, land use and management practices over a set period of time (Arnold *et al.*, 2012).

In SWAT, the watershed is divided into multiple sub-basins, which are further subdivided into hydrological response units (HRUs) consisting of homogeneous land-use management, slope and soil characteristics (Arnold *et al.*, 2012; Arnold *et al.*, 1998). HRUs are the smallest units of the watershed in which relevant hydrologic components such as evapo-transpiration,

surface run-off and peak rate of run-off, groundwater flow and sediment yield can be estimated. Water balance is the driving force behind all the processes in the SWAT calculated using eqn.7.

$$SW_t = SW_o + \sum_{I=1}^{t}(R_{day} - Q_{surf} - E_a - W_{seep} - Q_{gw}) \tag{7}$$

where SWt is the final soil water content (mm H_2O), SW_o is the initial soil water content on day i (mm H_2O), t is the time (days), R_{day} is the amount of precipitation on day i (mm H_2O), Q_{surf} is the amount of surface run-off on day i (mm H_2O), Ea is the amount of evapo-transpiration on day i (mm H_2O), W_{seep} is the amount of water entering the vadose zone from the soil profile on day i (mm H_2O), and Q_{gw} is the amount of return flow on day i (mm H_2O).

Run-off is calculated separately for each HRU and routed to obtain the total streamflow for the watershed using either the soil conservation service (SCS) curve number (CN) method (USDA, 1972) Figure 2. However, spatial connectivity and interactions among HRUs are ignored, instead, the cumulative output of each spatially discontinuous HRUs at the subwatershed outlet is directly routed to the channel (Pignotti et al., 2017). This lack of spatial connectivity among HRUs makes implementation and impact analysis of spatially-targeted management such as soil and water conservation structure difficult to incorporate in the model. To overcome this problem, efforts were made by different authors. For instance, a grid-based version of the SWAT model (Rathjens et al., 2015), landscape simulation on a regularized grid (Rathjens and Oppelt, 2012). Moreover, (Arnold et al., 2010) and (Bosch et al., 2010) further modify SWAT that allows landscapes to be subdivided into catenas comprised of upland, hillslope, and floodplain units and flow to be routed through these catenas. However, SWATgrid, developed to overcome this limitation, remains largely untested and computational demanding (Rathjens et al., 2015).

Hence, the standard SWAT CN method was chosen in this study because it is tested in many watersheds of Ethiopia such as (Gashaw *et al.*, 2018; Gebremicael *et al.*, 2013; Setegn *et al.*, 2008; Woldesenbet *et al.*, 2017b) and because of its ability to use daily input data (Arnold et al., 1998; Neitsch et al., 2011; Setegn et al., 2008) as compared to GAIM, which require sub daily precipitation as a model input that can be difficult to obtain in data scare region like UBNRB. This study focused on the effects of LULC and climate change on the water balance components of the basin, which includes the component of inflows, outflows and the change in storage. Precipitation is the main inflow, while evapo-transpiration (Et), surface run-off (Qs), lateral flow (Ql), and base flow (Qb) are the outflows. SWAT has three storages, namely, soil moisture (SM), shallow aquifer (SA) and deep aquifer (DA). Water movement from the soil moisture storage to the shallow aquifer is due to percolation, whereas, water movement from the shallow aquifer reverse upward to the soil moisture storage is Revap. For a more detailed description of the SWAT model, reference is made to Neitsch *et al.* (2011).

The SWAT model setup and data preparation can be done using arcSWAT tools in the arcGIS environment, while parameter sensitivity analysis, model calibration and validation was performed using the SWAT-CUP (Calibration and Uncertainty Procedures) interface Sequential Uncertainty Fitting (SUFI-2) algorithm (Abbaspour, 2008). During model setup, the observed daily weather and streamflow data of the given period was divided in to three different periods, the first to warm up the model, the second to calibrate the model and the third to validate the model. The first step in SWAT is the determination of the most sensitive parameters for a given watershed using global sensitivity analysis option (Arnold *et al.*, 2012). The second step is the calibration process adjusting the model input parameters necessary to match model output with observed data, thereby reducing the prediction uncertainty. Initial parameter estimates were taken from the default lower and upper bound values of the SWAT model database and from earlier studies in the basin e.g.(Gebremicael *et al.*, 2013). The final step, model validation involves running a model using parameters that were determined during the calibration process, and comparing the predictions to independent observed data not used in the calibration.

In this study both manual and automatic calibration strategies were applied to attain the minimum differences between observed and simulated streamflows in terms of surface flow, peak and total flow following the steps recommended by Arnold *et al.* (2012). For the purpose of impact analysis, we divided the simulation periods of (1971-2010) into four decadal periods, hereafter referred as the 1970s (1971-1980), 1980s (1981-1990), 1990s (1991-2000) and 2000s (2001-2010), as shown in Table 2. The models performance for the streamflow was then evaluated using statistical methods (Moriasi *et al.*, 2007) such as the Nash–Sutcliffe coefficient of efficiency (NSE), the coefficient of determination (R^2) and the relative volume error (RVE %), which are shown by eqn.8-10. Furthermore, graphical comparisons of the simulated and observed data, as well as water balance checks were used to evaluate the model's performance.

$$R^2 = \frac{[\sum(Q_{m,i} - \bar{Q}_m)(Q_{s,i} - \bar{Q}_s)]^2}{\sum(Q_{m,i} - \bar{Q}_m)^2 \sum Q_{s,i} - \bar{Q}_s^2} \tag{8}$$

$$NSE = 1 - \frac{\sum(Q_m - Q_s)_i^2}{(Q_{m,i} - \bar{Q}_m)^2} \tag{9}$$

$$RVE\ (\%) = 100 * \frac{\sum_{i=1}^{n}(Q_m - Q_s)_i}{\sum_{i=1}^{n} Q_{m,i}} \tag{10}$$

where $Q_{m,i}$ is the measured streamflow in m^3s^{-1}, Q_m is the mean values of the measured streamflow (m^3s^{-1}), $Q_{s,i}$ is the simulated streamflow in m^3s^{-1}, and Q_s is the mean values of simulated data in m^3s^{-1}.

4.4 SWAT simulations

In order to assess the individual and combined effects of LULC and climate change on streamflow and water balance components, three different approaches were applied . The first approach is to assess the response of streamflow to combined

LULC and climate change. We divided the analysis period (1971–2010) into four equal periods (four decade), periods when the hydrological regime within a catchment is expected to be changed due to land use changes (Marhaento *et al.*, 2017; Yin *et al.*, 2017b). The first period 1970s was regarded as the baseline period and the other periods 1980s, 1990s and 2000s were regarded as altered periods. LULC maps of 1973, 1985, 1995 and 2010 were used to represent the LULC patterns of the period 1970s , 1980s, 1990s and 2000s respectively. To analyze the response of streamflow and water balance components caused by the combined effects of LULC and climate change at decadal time periods, the SWAT model was separately calibrated and validated for each decades using the respective LULC map and weather data (Table 2). The DEM and soil data sets remained unchanged. The differences between the simulation result of the baseline and altered periods represent the combined effects of LULC and climate changes on streamflow and water balance components.

The second approach included simulations to attribute only for LULC changes, aimed to investigate whether LULC change is the main driver for changes in water balance components. To identify the hydrological impacts caused by LULC only, "A fixing -changing" method was used (Marhaento *et al.*, 2017; Woldesenbet *et al.*, 2017b; Yan *et al.*, 2013; Yin *et al.*, 2017a). The calibrated and validated SWAT model and its parameter settings in the baseline period was forced by weather data from the baseline period 1973-1980 while changing only the LULC maps of 1985, 1995, and 2010, keeping the DEM and soil data constant as suggested by (Hassaballah *et al.*; Marhaento *et al.*, 2017; Woldesenbet *et al.*, 2017b; Yin *et al.*, 2017a). We ran the calibrated SWAT model for the baseline period (1970s) four times changing only LULC map of the year 1973, 1985, 1995 and 2010 and remained constant weather data set of the 1970s(Table 2). The third approach is similar to the second approach but the simulations are attributed only for climate changes. A model was run again four times, corresponding to the LULC periods using a unique LULC map of the year 1973 but altering the four different periods of weather data sets (1970s, 1980s, 1990s and 2000s).

5. Results and discussions

5.1 Trend test

5.1.1 Rainfall

The summary of the MK trend tests result for the rainfall of the 15 selected stations located inside and around the UBNRB revealed a mixed trend (increasing, decreasing and no change). For daily time series, the computed probability values (p-value) for seven stations was greater while for eight stations it was less than the given significance level (α=5 %). This means no statistically significant trends existed in seven stations but a monotonic trend was occurred in the remaining 8 stations. Positive trends occurred only at 6 stations, of which 4 stations concentrated in the northern and central highlands (Bahirdar, Dangila, Debre Markos and G/bet), the other two stations (Assosa and Angergutten) are located in the south-west

and southern lowlands Figure 1. The other two stations, Alemketema and Nedjo respectively located in the East and South-West of UBNRB show a decreasing trend. On monthly basis, the MK trend test result showed that no statistically significant trend existed in all 15 stations. On an annual time scale, MK trend test could not find any trend in 11 stations while four stations (Alemketema, Debiremarkos, Gimijabet and Shambu) exhibited a trend. The trend analysis result of the annual rainfall time series has a good agreement with previous study by Gebremicael *et al.* (2013), who reported no significant change of annual rainfall in 8 out of 9 stations during the period 1973-2005. Hence, it is interesting to note that the time scale of analysis is critical factor to determine the given trends.

The basin wide rainfall trend and change point analysis was again carried out at daily, monthly, seasonal and annual time scale using MK test and Pettitt test respectively as summarized in Table 3 and Figure 3. The MK-test showed increasing trends for annual, monthly and long rainy season rainfall series while no trend for daily, short rainy and dry season rainfall series. The magnitude of trends for annual, monthly and long rainy season rainfall series are not significant as explained by the values of Sen's slope. However, the Pettitt test could not detect any jump point in basin wide rainfall series except for daily time series rainfall. .

Previous studies carried out the trend analysis of the basin-wide rainfall such as (Conway, 2000; Gebremicael *et al.*, 2013; Tesemma *et al.*, 2010), reported that no significant change of annual and seasonal rainfall series over the UBNRB. This disagreement could be due to the number of stations and their spatial distribution over the basin, time period of the analysis, approach used to calculate basin wide rainfall from gauging stations and sources of data. Tesemma et al. (2010) was used monthly rainfall data downloaded from Global Historical Climatology Network (NOAA, 2009) and the 10-day rainfall data for the 10 selected stations obtained from the National Meteorological Service Agency of Ethiopia from 1963-2003. Conway (2000) was also constructed basin-wide annual rainfall of UBNRB for the period 1900-1998 from the mean of 11 gauges. Furthermore, (Conway, 2000) employed simple linear regressions over time to detect trends in annual rainfall series without removing the serial autocorrelation effects. Gebremicael *et al.* (2013), also used only 9 stations from the period 1970-2005. However, in this study, we used daily observed rainfall data from 15 stations collected from Ethiopian Meteorological Agency from 1971-2010. The stations are more or less evenly spatially distributed over UBNRB. We applied widely used spatial interpolation technique (Thiessen polygon method) to calculate basin-wide rainfall series from station data.

5.1.2 Streamflow

The result of MK-test for daily, monthly, annual and seasonal (long and short rainy season and dry season) time series streamflow showed a positive trend and the trend magnitude is statistically significant as summarised in Table 3. Meanwhile, the Pettitt test detects change point for daily, annual and short rainy season streamflows but cannot detect change point for monthly, long and dry season streamflows Figure 3. The change point detected by Pettitt test for annual rainfall series is

occurred in 1995 while for daily and dry seasons are respectively in 1985 and 1987. The result obtained from MK test has a good agreement with the previous study carried out by Gebremicael et al. (2013), which reported an increasing trend in the observed annual, short and long rain seasons streamflow at the El Diem gauging station but disagree with the result of dry season streamflow. Furthermore, the increasing trend of long rainy season streamflow well agree with the result of Tesemma et al. (2010), but disagree with the results of short rainy season and annual flows. (Tesemma et al., 2010), reported that the short rainy season and the annual flows are constant for the analysed period of 1964–2003. This disagreement is likely attributed to the difference of analysis period as can be seen from Figure 3, the last seven years (2004–2010) had relatively higher streamflow records.

Although, the results of MK test for the annual and long rainy season rainfall and streamflow show increasing trend for the last 40 years in the UBNRB, the magnitude of Sen's slope for streamflow is much larger than the Sen's slope of rainfall (Table 3). Moreover, for the short rainy season streamflow shows statistically significant positive increasing while the rainfall shows no change. The mismatch of trend magnitude between rainfall and streamflow could be attributed to the combined effect of LULC and climate change, associated with evapotranspiration, infiltration rate by changing soil properties rainfall intensity and extreme events.

5.2 LULC change analysis

According to the confusion matrix report, overall accuracy of 80 %, producer's accuracy values for all classes ranged from 75.4 % to 100 %, user's accuracy values ranged from 83.7 % to 91.7 % and the kappa coefficient (k) of 0.77 were attained for the 2010 classified image as shown in Table 5. Monserud (1990) suggested a kappa value of <40 % as poor, 40–55 % fair, 55–70 % good, 70–85 % very good and >85 % as excellent. According to these ranges, the classification in this study has very good agreement with the validation data set and met the minimum accuracy requirements to be used for further change detection and impact analysis.

The classified images of the basin (Figure 4) have shown different LULC proportion at four different time periods as shown in Figure 5. In 1973, the UBNRB was dominated by cultivated land (62.9 %), followed by bushes & shrubs (18 %), forest (17.4 %), and water (1.74 %). In 1985, the cultivated land increased to (65.6 %), followed by bushes & shrubs (18.3 %), while forest decreased to (14.4 %), and water remained unchanged at (1.7 %). In 1995, cultivated land further increased to (67.5 %), followed by bushes & shrubs (18.5 %), forest further decreased (to 12.2 %), and water remained unchanged (1.7 %). In 2010, cultivated land decreased to (63.9 %), bushes and shrubs increased to (18.8 %), forest increased to (15.6 %) and water remained unchanged at (1.7 %). During the entire 1973–2010 period, cultivated land, along with bushes & shrubs remained the major proportions as compared to the other LULC classes. The highest gain (2.7 %) and the largest loss (-3.6 %) in cultivated land occurred during the 1973–1985 and 1995-2010 periods respectively. The highest gain in bushes and

shrubs was (0.3 %) from 1973 to 1985, while the highest gain in forest coverage (3.4 %) was recorded during the period 1995–2010. Water coverage remained unchanged from 1973 to 2010.

Although, the image classification has very good accuracy, uncertainties could be expected for the following reasons. Firstly, as elsewhere in Ethiopia, LULCs change rapidly over space, and image reflectance may be confusing due to the topography and variation in the image acquisition date. Landsat images were not all available for one particular year or one season; thus images came from a mix of years, and from a variety of seasons might have errors. Secondly, the workflow associated with LULC classification, which involve many steps and can be a source of uncertainty. The errors are observed in the classified LULC map as shown in Figure 4. In Figure 4 (a) on the western side of the map is a rectangular section with forest, that completely disappears in 4(b). In 4(b) there is a rectangular forest cover in the northern part of the country which again disappears completely in 4(c). In 4(d) a forest cover with linear edges (North-South) appears on the eastern side of the map. That being recognised, overall the land cover mapping is reasonably accurate, providing a good base for land cover estimation and for providing basic information for the objective of hydrological impact analysis.

The rate of expansion of cultivated land before 1995 was high as compared to after 1995. Conversely, the area devoted to forest land decreased in the 1985 and 1995 from the baseline 1973. However, after 1995, the forest began to increase while the cultivated land decreased. The increased forest coverage and the reduction in cultivated land over the period 1995 to 2010 showed that the environment was recovering from the devastating drought and forest clearing for firewood and cultivation due to population growth has minimized. This could be due to the afforestation programme initiated by the Ethiopian government and due to the extensive soil and water conservation measure carried out by the community. Since 1995, eucalyptus tree plantation expanded significantly across the country at homestead level for fire wood, construction material, for producing charcoal and for generating income (Woldesenbet *et al.*, 2017b). To summarize, in the period 2010, forest coverage declined by 1.8 %, with increasing of both bushes and shrubs, as well as cultivated land by 0.8 % and 1 % respectively from the original 1973 level. This result agrees well with other studies (Gebremicael *et al.*, 2013; Rientjes *et al.*, 2011; Teferi *et al.*, 2013; Woldesenbet *et al.*, 2017b), who reported the a significant conversion of natural vegetation cover into agricultural land.

5.3 SWAT model calibration and validation

The most sensitive parameters of the SWAT model to simulate streamflow were identified using global sensitivity analysis of SWAT-CUP and their optimized values were determined by the calibration process recommended by Arnold *et al.* (2012). Parameters such as SCS curve number (CN2), base flow alpha factor (ALPHA_BF), soil evaporation compensation factor (ESCO), threshold water depth in the shallow aquifer required for return flow to occur (GWQMN), groundwater "revap"

coefficient (GW_REVAP) and the available water capacity (SOL_AWC) were found to be the most sensitive parameters for the flow predictions.

Figure 6 shows the calibration and the validation results of monthly streamflow hydrographs and this result revealed the model well captured the monthly hydrographs. This was again verified by the statistical performance measures of R^2, NSE and RVE (%) as presented in Table 6. For the calibration period, the values of R^2, NSE and RVE (%) from the four model is ranged from 0.79 to 0.91, 0.74 to 0.91 and -3.4 % to 4 % and for the validation period it ranged from 0.84 to 0.94, 0.82 to 0.92 and -7.5 % to 7.4 % respectively. According to the rating of Moriasi *et al.* (2007), the performance of the SWAT model over UBNRB can be categorized as very good, although underestimation was observed in the base flow simulation. The optimal parameter values of the calibrated four model runs are shown in Table 7. A change was obtained for CN2 parameter values, which can be attributed to the catchment response behaviour. For instance, an increase in the CN2 value in the 1980s and 1990s from 0.89 to 0.91 and 0.92 as compared to 1970s respectively, indicate a reduction in forest coverage and expansion of cultivated land. In contrary, a decrease in CN2 value was attained during the period 1990s to 2000s from 0.92 to 0.9, attributed to the increase in forest coverage and reduction in cultivated land.

5.4 Effects of combined LULC and climate change on streamflow and water balance components

The simulation result of the four independent decadal time scale calibrated and validated SWAT model runs indicate the combined effect of both LULC and climate change during the last 40 years' time (Table 8). From the simulation result, mean annual streamflow increased by 16.9 % between the period 1970s and the 2000s. However, the rate of change is different in different decades. For example, it increased by 3.4 % and 9.9 % during the period 1980s and 1990s respectively from the baseline period 1970s.

The ration of mean annual streamflow to mean annual precipitation (Qt/P) increased from 19.4 % to 22.1 %, and actual evaporation to precipitation (Ea/P) decreased from 61.1 % to 60.5 % from the 1970s to 2000s. Moreover, the ration of surface run-off to streamflow (Qs/Qt) has significantly increased from 40.7 % to 50.1 % and 55.4 % in the 1980s and 1990s respectively and decreased to 43.7 % in the 2000s. In contrast, the base flow to streamflow ration (Qb/Qt) has significantly decreased from 17.1 % to 10.3 % and 3.2 % respectively during the period 1980s and 1990s but has increased to 20 % in the period 2000s. The result for surface runoff agrees with the previous study done by (Gebremicael et al., 2013) but disagree for baseflow. They reported surface runoff (Qs) contribution to the total river discharge has increased by 75%, while the baseflow (Qb) flow has decreased by 50% from the period 1970s to 2000s. This indicate that 1.8 % forest cover loss and 1 % increased cultivated land combined with 2.2 % increased rainfall from the 1970s to the 2000s led to a 16.9 % increase in simulated streamflow. 1990s was the period when the highest deforestation and expansion of cultivated land reported; meanwhile it is the time when the rainfall intensity and number of rainfall events has significantly increased compared to the 1970s and 1980s, as shown in Table 4. Hence, the increased mean annual streamflow could be ascribed to the combined

effects of LULC and climate change. In the case of (Qs/Qt), the increasing pattern could be ascribed to the increasing of rainfall intensities and expansion of cultivated land and decreasing of forest coverage, which might adversely affect soil water storage, and decrease rainfall infiltration, thereby increase water yield or streamflow. In contrary, the decreasing of (Qb/Qt) has positive relation with the increasing of evapotranspiration linked to both LULC and climate factors (Table 8).

5   This hypothesis can be explained with the change in CN2 parameter values obtained during the calibration of the four SWAT model runs.

The CN2 parameter value which is a function of evapotranspiration derived from LULC, soil type, and slope, increased in the 1980s and 1990s from 1970s could be associated with the expansion of cultivated land and shrinkage of forest land. The

10   increasing of CN2 results to generate more surface runoff and less baseflow. Another important contributing factor for the decreasing of surface run-off and increasing of base flow ration in the 2000s from 1990s could be the placement of soil and water conservation (SWC) measures. According to Haregeweyn et al. (2015), various nationwide SWC initiatives have been undertaken since the 1980s such as Food-for-Work (FFW) (1973–2002), Managing Environmental Resources to Enable Transition to more sustainable livelihoods (MERET, 2003–2015), Productive Safety Net Programs (PSNP, 2005–present),

15   Community Mobilization through free-labor days (1998–present), and the National Sustainable Land Management Project (SLMP, 2008–2018). The effectiveness of the initiatives were evaluated by (Haregeweyn *et al.*, 2015) and come up with the conclusion that community labour mobilization seems to be the best approach. It can reduce a mean seasonal surface run-off by 40 %, with large spatial variability, ranging from 4 % in Andit Tid (northwest Ethiopia) to 62 % in Gununo (south Ethiopia).

5.5 Effects of a single change in LULC on streamflow and water balance components

To identify the hydrological impacts caused by LULC only, "A fixing -changing" method was used (Yan *et al.*, 2013). The calibrated and validated SWAT model and its parameter settings in the baseline period was forced by weather data from the baseline period 1973-1980 while changing only the LULC maps from 1985, 1995, and 2010, keeping the DEM and soil data

25   constant as suggested by (Hassaballah et al.). The result from Figure 7 indicated that Qs/Qt ratio changed from 40.7 % to 41.2 %, 41.1 % and 40.9 % respectively by using the LULC maps from 1973, 1985, 1995 and 2010 whereas the Qb/Qt ratio changed from 17.1 % to 16.8 %, 16.5 % and 16.9 % respectively. The highest Qs/Qt ratio (41.9 %) and the lowest Qb/Qt ratio (16.5 %) was recorded with the LULC map of 1995. This could be attributed to the 5.1 % reduction in forest coverage and 4.6 % increase in cultivated land with the 1995 LULC map as compared to the 1973 LULC map.

On a basin scale, over a decadal time period, water gains mainly from precipitation, and the losses are mainly due to run-off and evapotranspiration (Oki *et al.*, 2006). In the fixing-changing approach, the change in streamflow due to LULC was essentially the change in the evapotranspiration between the two periods, as the amount of precipitation was constant (1970s)

and the change in the water storage during the two periods was similar (Yan et al., 2013). The annual Ea losses from seasonal crops are smaller than Ea losses from forests, as seasonal crops only transpire relatively shorter time period than perennial trees transpire (Yan et al., 2013). As a result, actual mean annual evapotranspiration (Ea) simulated by SWAT model was 871.6 mm at the baseline. It decreased to 871.4 mm and 871 mm in the 1985 and 1995 respectively and increased to 872.1 mm in the 2010. This could be due to simultaneous expansion of cultivated land and shrinkage in forest coverage in the LULC map of 1985 and 1995 from the base line 1973. Furthermore, this deforestation may cause a reduction in canopy interception of the rainfall, decreases the soil infiltration by increasing raindrop impacts and reduce plant transpiration which can significantly increase surface run-off and reducing base flow (Huang et al., 2013). Here, the change of evapotranspiration caused by the LULC change is minimal as a result the change for surface runoff and baseflow is not significant.

5.6 Effects of single climate change on streamflow and water balance components

The impacts of climate change are analysed by running the four models using a unique LULC map of 1973 with its model parameters while changing only the weather data sets from 1970s, 1980s, 1990s and 2000s. The simulated water balance components shown in Figure 7, indicate that the Qs/Qt ratio increased from 40.7 % to 45.2 %, 45.6 % and 46.2 % during the period 1970s, 1980s, 1990s and 2000s respectively, while, the Qb/Qt ratio changed from 17.1 % to 13.5 %, 14.9 % and 12.7 % for the same simulation periods. The decreasing of the ratio of (Qb/Qt) for the altered periods as compared to the baseline period could be attributed to the increasing of evapotranspiration from 872 to 854, 906 and 884 mm respectively in 1970s, 1980s, 1990s and 2000s which can be linked to temperature and amount of rainfall. However, it is important to know the dominant rainfall-runoff process of the study area to fully understand the effect of climate change on the water balance components.

Although, there is no any detail research carried out on the Blue Nile basin to investigate about the runoff generation processes, Liu et al. (2008) investigated the rainfall-runoff processes at three small watersheds located inside and around Upper Blue Nile basin, namely: Mayber, AnditTid and Anjeni. Their analysis showed that, unlike in temperate watersheds, in monsoonal climates, a given rainfall volume at the onset of the monsoon produces a different run-off volume than the same rainfall at the end of the monsoon. Liu et al. (2008) and Steenhuis et al. (2009) showed that the ratio of discharge to precipitation minus evapotranspiration (Q/(P- ET)) increases with cumulative precipitation from the onset of monsoon. This suggesting that saturation excess processes play an important role in watershed response.

Furthermore, the infiltration rates measured in 2008 by Engda (2009) were compared with rainfall intensities in the Maybar and Andit Tid watersheds located inside and around UBNRB. In Andit Tid watershed, which has an area of less than 500 ha, the measured infiltration rates at 10 locations were compared with rainfall intensities considered from the period 1986-2004. The analysis showed that only 7.8 % of rainfall intensities were found higher than the lowest soil infiltration rate of 2.5

cm hr^{-1}. A similar analysis was performed by Derib (2005) in the Maybar watershed (with a catchment area of 113 ha). The infiltration rates measured from 16 measurements were ranged from 19 to 600 mm hr^{-1}with an average value of 24 cm hr^{-1} and the median was 18 cmhr^{-1} while the average daily rainfall intensity from 1996 to 2004 was 8.5 mm hr^{-1}. Hence, from these infiltration measurements, he suggested that infiltration excess run-off is not a common feature in these watersheds.

From the above discussion points, it is to be noted that surface runoff could increase with the increasing of total rainfall amount regardless of rainfall intensity. However, in this study, the mean annual rainfall amount was decreasing from 1970s to 1980s (1428 and 1397 mm respectively) while the (Qs/Qt) ratio increased from 40.7 % to 45.2 %. Similarly, the mean annual rainfall amount in 1990s (1522 mm) was higher than the mean annual rainfall amount in 2000s (1462 mm) while the

10 (Qs/Qt) increased from 45.6 % to 46.2 %. In contrary, climate indexes such as 99-percentile rainfall, SDII (ratio of total precipitation amount to R1mm) and R20mm are increasing consistently from the period 1970 to 2000s as shown in Table 4. This indicates that the increasing of surface run-off might be due to increasing of rainfall extreme events and rainfall intensity. In other words, this study revealed that infiltration excess of overland flow dominates rainfall-runoff processes in the UBNRB not for saturation excess of overland flow. The contradiction from the previous studies might be either due to

15 the limitation of SWAT- CN method when applied in monsoonal climates or due to the overlooked of tillage activities which has significant impact on the soil infiltration rate by the previous studies. At the beginning of the rainy season, extensive tillage activities carried out across the basin, as a result soils get disturbed which can increase infiltration rate and finally decrease the amount of rainfall converted to runoff.

20 Although, the CN method is easy to use, provides acceptable results in many cases for discharge at the watershed outlet, researchers have concerns over its use in watershed models (Steenhuis et al., 1995; White et al., 2011). SWAT-CN model relies with a statistical relationship between soil moisture condition and CN value obtained from plot data in the United States with a temperate climate that was never tested in monsoonal climate where two extreme soil moisture conditions exhibited. In monsoonal climates, long period of rain can lead to prolonged soil saturation while during the dry period the

25 soil dries out completely which may not happen in temperate climates (Steenhuis *et al.*, 2009). Hence, further research is necessary that considers bio-physical activities such as tillage and seasonal effects to soil moisture at representative watersheds of the basin for assessing the rainfall-runoff processes properly.

6. Conclusions

30 The objectives of this study were to understand the long-term variations of rainfall and streamflow of the UBNRB using statistical techniques (MK and Pettitt tests), and to assess the combined and single effects of climate and LULC change using a semi-distributed hydrological model (SWAT). Although, the results of MK test for the annual and long rainy season rainfall and streamflow show increasing trend for the last 40 years in the UBNRB, the magnitude of Sen's slope for

streamflow is much larger than the Sen's slope of areal rainfall. Moreover, for the short rainy season streamflow shows statistically significant positive increasing while the rainfall shows no change. The mismatch of trend magnitude between rainfall and streamflow could be attributed to the combined effect of LULC and climate change, associated with decreasing actual evapotranspiration (Ea) and increasing rainfall intensity and extreme events.

The LULC change detection was assessed by comparing the classified images and the result showed that the dominant process is largely the expansion of cultivated land and decrease in forest coverage. The rate of deforestation is high during the period 1973-1995, this is probably due to the severe drought occurred in mid 1980s and due to large population increase as a result expansion of agricultural land. On the other hand, forest coverage increased by 3.4 % during the period 1995 to

10   2010. This indicates that the environment was recovering from the devastating drought of 1980s and regenerating of forests as the result of afforestation programme initiated by the Ethiopian government and due to soil and water conservation activities done by the communities.

The SWAT model was used to analyse the combined and single effects of LULC and climate changes on the monthly

15   streamflow at the basin outlet (El Diem station, located on the Ethiopia-Sudan border). The result showed that the combined effects of the LULC and climate changes increased the mean annual streamflow by 16.9 % from the 1970s to the 2000s. The increased mean annual streamflow could be ascribed to the combined effects of LULC and climate change. The LULC change alters the catchment responses as a result SWAT model parameter values could be changed. For instance, the expansion of cultivation land and the shrinkage of forest coverage from 1973 to 1995 has changed the CN2 parameter values

20   from 0.89 in 1973 to 0.91 and 0.92 in the 1985 and 1995 respectively. The increasing of CN2 value might increase surface run-off and decrease base flow. Similarly, the increase in rainfall intensity and extreme precipitation events led to a substantial increase in Qs/Qt and a substantial decrease in Qb/Qt and ultimately increases in the streamflow during the 1971-2010 simulation period.

25   The "fixing-changing" approach result using SWAT model revealed that the single effect of LULC change could potentially altered the streamflow generation processes. Expansion of cultivated land might reduce evapotranspiration because transpiration for seasonal crops is less than the transpiration of perennial trees (Yan et al., 2013) as a result surface run-off increased. Alternatively, reduction of forest coverage may cause a reduction in canopy interception of the rainfall, decrease the soil infiltration by increasing raindrop impacts and reduce plant transpiration which can significantly increase surface

30   run-off and reducing base flow (Huang et al., 2013). In general, 5.1 % reduction in forest coverage and 4.6 % increase in cultivated land led to 9.9 % increase of mean annual streamflow from 1973 to 1995. This study provides a better understanding and substantial information how climate and LULC change affects streamflow and water balance components separately and jointly, which is useful for basin-wide water resources management. The SWAT simulation indicated that the impacts of climate change is substantial as compared to the impacts of LULC change as it is shown in Figure 7. Surface

water is not any more used for agriculture and plant consumption in areas where there is limited water storage facilities like UBNRB where as base flow is the reliable sources for irrigation to increase agricultural production. Hence, the increasing of surface water and reduction of base flow caused by both LULC and climate changes negatively affects the socio-economic developments of the basin.

Therefore, protecting and conserving the natural forests and expanding soil and water conservation activities are highly recommended, not only for increasing the base flow available for irrigation but also reducing soil erosion. By doing so, the productivity might be increased, livelihoods and regional water resource use cooperation might be improved. However, this study might have limitations due to the uncertainties of Landsat image classification and the simulation of SWAT model. In

10 order to improve the accuracy of LULC classification from Landsat images, further efforts such as the integration of other images together with Landsat images through image fusion techniques (Ghassemian, 2016) is required. The SWAT model does not adjust CN2 for slopes greater than 5%, which could be significant in areas where the majority of the area has a slope greater than 5%, such as UBNRB. Therefore, we suggest adjusting the CN2 values for slope > 5 % outside of the SWAT model might improve the results. Moreover, further research that involves rainfall intensity, infiltration rate and

15 event-based analysis of hydrographs and critical evaluation of rainfall-runoff processes in the study area might improve the limitation of this study. Finally, the authors would like to point out that the impacts of current and future water resource developments should be investigated in order to establish comprehensive and holistic water resource management in the Nile basin.

References

20 Abbaspour, C.K., 2008. SWAT Calibrating and Uncertainty Programs. A User Manual. Eawag Zurich, Switzerland.
Allen, R.G., Pereira, L.S., Raes, D., Smith, M., 1998. Crop evapotranspiration-Guidelines for computing crop water requirements-FAO Irrigation and drainage paper 56. FAO, Rome, 300(9): D05109.
Arnold, J., Allen, P., Volk, M., Williams, J., Bosch, D., 2010. Assessment of different representations of spatial variability on SWAT model performance. Transactions of the ASABE, 53(5): 1433-1443.
25 Arnold, J.G., Moriasi, D.N., Gassman, P.W., Abbaspour, K.C., White, M.J., Srinivasan, R., Santhi, C., Harmel, R., Van Griensven, A., Van Liew, M.W., 2012. SWAT: Model use, calibration, and validation. Transactions of the ASABE, 55(4): 1491-1508.
Arnold, J.G., Srinivasan, R., Muttiah, R.S., Williams, J.R., 1998. Large area hydrologic modeling and assessment part I: Model development1. Wiley Online Library.
30 Awulachew, S.B., McCartney, M., Steenhuis, T.S., Ahmed, A.A., 2009. A review of hydrology, sediment and water resource use in the Blue Nile Basin, 131. IWMI.
Banko, G., 1998. A review of assessing the accuracy of classifications of remotely sensed data and of methods including remote sensing data in forest inventory.
BCEOM, 1998. Abbay river basin integrated development master plan project.

Bewket, W., Sterk, G., 2005. Dynamics in land cover and its effect on stream flow in the Chemoga watershed, Blue Nile basin, Ethiopia. Hydrological Processes, 19(2): 445-458.

Bosch, D., Arnold, J., Volk, M., Allen, P., 2010. Simulation of a low-gradient coastal plain watershed using the SWAT landscape model. Transactions of the ASABE, 53(5): 1445-1456.

Cheung, W.H., Senay, G.B., Singh, A., 2008. Trends and spatial distribution of annual and seasonal rainfall in Ethiopia. International Journal of Climatology, 28(13): 1723-1734.

Congalton, R.G., 1991. A review of assessing the accuracy of classifications of remotely sensed data. Remote sensing of environment, 37(1): 35-46.

Conway, D., 2000. The climate and hydrology of the Upper Blue Nile River. The Geographical Journal, 166(1): 49-62.

DeFries, R., Chan, J.C.-W., 2000. Multiple criteria for evaluating machine learning algorithms for land cover classification from satellite data. Remote Sensing of Environment, 74(3): 503-515.

Derib, S.D., 2005. Rainfall-runoff processes at a hill-slope watershed: case of simple models evaluation at Kori-Sheleko Catchments of Wollo, Ethiopia, M. Sc. Thesis.

Engda, T.A., 2009. Modeling rainfall, runoff and soil loss relationships in the northeastern highlands of Ethiopia, andit tid watershed, Citeseer.

Gashaw, T., Tulu, T., Argaw, M., Worqlul, A.W., 2018. Modeling the hydrological impacts of land use/land cover changes in the Andassa watershed, Blue Nile Basin, Ethiopia. Science of The Total Environment, 619: 1394-1408.

Gebremicael, T., Mohamed, Y., Betrie, G., van der Zaag, P., Teferi, E., 2013. Trend analysis of runoff and sediment fluxes in the Upper Blue Nile basin: A combined analysis of statistical tests, physically-based models and landuse maps. Journal of Hydrology, 482: 57-68.

Ghassemian, H., 2016. A review of remote sensing image fusion methods. Information Fusion, 32: 75-89.

Hamed, K.H., Rao, A.R., 1998. A modified Mann-Kendall trend test for autocorrelated data. Journal of Hydrology, 204(1-4): 182-196.

Haregeweyn, N., Tsunekawa, A., Nyssen, J., Poesen, J., Tsubo, M., Tsegaye Meshesha, D., Schütt, B., Adgo, E., Tegegne, F., 2015. Soil erosion and conservation in Ethiopia: a review. Progress in Physical Geography, 39(6): 750-774.

Hassaballah, K., Mohamed, Y., Uhlenbrook, S., Biro, K., Analysis of streamflow response to land use land cover changes using satellite data and hydrological modelling: case study of Dinder and Rahad tributaries of the Blue Nile (Ethiopia/Sudan).

Hayes, D.J., Sader, S.A., 2001. Comparison of change-detection techniques for monitoring tropical forest clearing and vegetation regrowth in a time series. Photogrammetric engineering and remote sensing, 67(9): 1067-1075.

Hu, Y., De Jong, S., Sluiter, R., 2004. A modeling-based threshold approach to derive change/no change information over vegetation area, Proceedings of the "12 International Conference on Geoinformatics-Geospatial Information Research: Bridging the Pacific and Atlantic". University of Gävle (Sweden), pp. 647-654.

Huang, J., Wu, P., Zhao, X., 2013. Effects of rainfall intensity, underlying surface and slope gradient on soil infiltration under simulated rainfall experiments. Catena, 104: 93-102.

Jensen, J.R., 1996. Introductory digital image processing: a remote sensing perspective. Prentice-Hall Inc.

Kendall, M., 1975. Rank correlation methods.

Liu, B.M., Collick, A.S., Zeleke, G., Adgo, E., Easton, Z.M., Steenhuis, T.S., 2008. Rainfall-discharge relationships for a monsoonal climate in the Ethiopian highlands. Hydrological Processes, 22(7): 1059-1067.

Lu, D., Mausel, P., Batistella, M., Moran, E., 2004. Comparison of land-cover classification methods in the Brazilian Amazon Basin. Photogrammetric engineering & remote sensing, 70(6): 723-731.

Mancino, G., Nolè, A., Ripullone, F., Ferrara, A., 2014. Landsat TM imagery and NDVI differencing to detect vegetation change: assessing natural forest expansion in Basilicata, southern Italy. iForest-Biogeosciences and Forestry, 7(2): 75.

Mann, H.B., 1945. Nonparametric Tests Against Trend. Econometrica, 13(3): 245-259.

Marhaento, H., Booij, M.J., Rientjes, T., Hoekstra, A.Y., 2017. Attribution of changes in the water balance of a tropical catchment to land use change using the SWAT model. Hydrological Processes, 31(11): 2029-2040.

McCartney, M., Alemayehu, T., Easton, Z.M., Awulachew, S.B., 2012. Simulating current and future water resources development in the Blue Nile River Basin. The Nile River Basin: water, agriculture, governance and livelihoods. Routledge-Earthscan, Abingdon: 269-291.

Mekonnen, D.F., Disse, M., 2018. Analyzing the future climate change of Upper Blue Nile River basin using statistical downscaling techniques. Hydrology and Earth System Sciences, 22(4): 2391.

Melesse, A., Abtew, W., Dessalegne, T., Wang, X., 2009. Low and high flow analyses and wavelet application for characterization of the Blue Nile River system. Hydrological processes, 24(3): 241.

Mengistu, D., Bewket, W., Lal, R., 2014. Recent spatiotemporal temperature and rainfall variability and trends over the Upper Blue Nile River Basin, Ethiopia. International Journal of Climatology, 34(7): 2278-2292.

Monserud, R.A., 1990. Methods for comparing global vegetation maps.

Moriasi, D.N., Arnold, J.G., Van Liew, M.W., Bingner, R.L., Harmel, R.D., Veith, T.L., 2007. Model evaluation guidelines for systematic quantification of accuracy in watershed simulations. Trans. Asabe, 50(3): 885-900.

Neitsch, S., Arnold, J., Kiniry, J.e.a., Srinivasan, R., Williams, J., 2002. Soil and water assessment tool user's manual version 2000. GSWRL report, 202(02-06).

Neitsch, S.L., Arnold, J.G., Kiniry, J.R., Williams, J.R., 2011. Soil and water assessment tool theoretical documentation version 2009, Texas Water Resources Institute.

NMA, 2013. Annual climate buletien for the year 2013.

Oki, T., Kanae, S., 2006. Global hydrological cycles and world water resources. science, 313(5790): 1068-1072.

Pettitt, A., 1979. A non-parametric approach to the change-point problem. Applied statistics: 126-135.

Pignotti, G., Rathjens, H., Cibin, R., Chaubey, I., Crawford, M., 2017. Comparative Analysis of HRU and Grid-Based SWAT Models. Water, 9(4): 272.

Polanco, E.I., Fleifle, A., Ludwig, R., Disse, M., 2017. Improving SWAT model performance in the upper Blue Nile Basin using meteorological data integration and subcatchment discretization. Hydrology and Earth System Sciences, 21(9): 4907.

Rathjens, H., Oppelt, N., 2012. SWATgrid: An interface for setting up SWAT in a grid-based discretization scheme. Computers & geosciences, 45: 161-167.

Rathjens, H., Oppelt, N., Bosch, D., Arnold, J.G., Volk, M., 2015. Development of a grid-based version of the SWAT landscape model. Hydrological processes, 29(6): 900-914.

Rientjes, T., Haile, A., Kebede, E., Mannaerts, C., Habib, E., Steenhuis, T., 2011. Changes in land cover, rainfall and stream flow in Upper Gilgel Abbay catchment, Blue Nile basin-Ethiopia. Hydrology and Earth System Sciences, 15(6): 1979.

Seleshi, Y., Zanke, U., 2004. Recent changes in rainfall and rainy days in Ethiopia. International journal of climatology, 24(8): 973-983.

Sen, P.K., 1968. Estimates of the regression coefficient based on Kendall's tau. Journal of the American statistical association, 63(324): 1379-1389.

Setegn, S.G., Srinivasan, R., Dargahi, B., 2008. Hydrological modelling in the Lake Tana Basin, Ethiopia using SWAT model. The Open Hydrology Journal, 2(1).

Singb, A., 1989. Digital change detection techniques using remotelyWsensed data. International Journal of Remote Sensing, 10(6): 989L1003.

Singh, A., 1989. Review article digital change detection techniques using remotely-sensed data. International journal of remote sensing, 10(6): 989-1003.

Steenhuis, T.S., Collick, A.S., Easton, Z.M., Leggesse, E.S., Bayabil, H.K., White, E.D., Awulachew, S.B., Adgo, E., Ahmed, A.A., 2009. Predicting discharge and sediment for the Abay (Blue Nile) with a simple model. Hydrological processes, 23(26): 3728-3737.

Steenhuis, T.S., Winchell, M., Rossing, J., Zollweg, J.A., Walter, M.F., 1995. SCS runoff equation revisited for variable-source runoff areas. Journal of Irrigation and Drainage Engineering, 121(3): 234-238.

Teferi, E., Bewket, W., Uhlenbrook, S., Wenninger, J., 2013. Understanding recent land use and land cover dynamics in the source region of the Upper Blue Nile, Ethiopia: Spatially explicit statistical modeling of systematic transitions. Agriculture, ecosystems & environment, 165: 98-117.

Tekleab, S., Mohamed, Y., Uhlenbrook, S., Wenninger, J., 2014. Hydrologic responses to land cover change: the case of Jedeb mesoscale catchment, Abay/Upper Blue Nile basin, Ethiopia. Hydrological Processes, 28(20): 5149-5161.

Tesemma, Z.K., Mohamed, Y.A., Steenhuis, T.S., 2010. Trends in rainfall and runoff in the Blue Nile Basin: 1964–2003. Hydrological processes, 24(25): 3747-3758.

Uhlenbrook, S., Mohamed, Y., Gragne, A., 2010. Analyzing catchment behavior through catchment modeling in the Gilgel Abay, upper Blue Nile River basin, Ethiopia. Hydrology and Earth System Sciences, 14(10): 2153-2165.

USDA, 1972. SCS national engineering handbook, section 4: hydrology. The Service.

von Storch, H., 1995. Misuses of Statistical Analysis in Climate Research, Analysis of Climate Variability. Springer, pp. 11-26.

White, E.D., Easton, Z.M., Fuka, D.R., Collick, A.S., Adgo, E., McCartney, M., Awulachew, S.B., Selassie, Y.G., Steenhuis, T.S., 2011. Development and application of a physically based landscape water balance in the SWAT model. Hydrological Processes, 25(6): 915-925.

Woldesenbet, T.A., Elagib, N.A., Ribbe, L., Heinrich, J., 2017a. Gap filling and homogenization of climatological datasets in the headwater region of the Upper Blue Nile Basin, Ethiopia. International Journal of Climatology, 37(4): 2122-2140.

Woldesenbet, T.A., Elagib, N.A., Ribbe, L., Heinrich, J., 2017b. Hydrological responses to land use/cover changes in the source region of the Upper Blue Nile Basin, Ethiopia. Science of the Total Environment, 575: 724-741.

Yan, B., Fang, N., Zhang, P., Shi, Z., 2013. Impacts of land use change on watershed streamflow and sediment yield: an assessment using hydrologic modelling and partial least squares regression. Journal of Hydrology, 484: 26-37.

Yin, J., He, F., Xiong, Y.J., Qiu, G.Y., 2017a. Effects of land use/land cover and climate changes on surface runoff in a semi-humid and semi-arid transition zone in northwest China. Hydrology and Earth System Sciences, 21(1): 183-196.

Yin, J., He, F., Xiong, Y.J., Qiu, G.Y., 2017b. Effects of land use/land cover and climate changes on surface runoff in a semi-humid and semi-arid transition zone in northwest China. Hydrology and Earth System Sciences, 21(1): 183.

Yue, S., Pilon, P., Phinney, B., Cavadias, G., 2002. The influence of autocorrelation on the ability to detect trend in hydrological series. Hydrological Processes, 16(9): 1807-1829.

Yue, S., Wang, C., 2004. The Mann-Kendall test modified by effective sample size to detect trend in serially correlated hydrological series. Water Resources Management, 18(3): 201-218.

Table 1: Areal long term (1971-2010) mean annual and seasonal rainfall and streamflow of UBNRB

Station	Amount				Contribution (%)				
	Kiremit	Belg	Bega	Total	Kiremit	Belg	Bega	Mean	Area (km^2)
Flow (m^{3}s^{-1})	3506.3	300.4	1018.4	4825.1	72.7	6.2	21.1	1608	172,254
Flow (BCM)	36.4	3.1	10.6	50.7					
Rainfall (mm)	1070.1	140.8	238.9	1449.8	73.8	9.7	16.5		

Kiremit: long rainy season, Belg: Short rainy season, Bega: Dry season

Table 2: Data sets for the baseline and altered periods for the SWAT simulation used to analyse the combined and single effect of LULC and climate changes on streamflow and water balance components

Model run No.	Combined effect		Isolated LULC change effect		Isolated climate change effect		Remark
	Climate data set	LULC map	Climate data set	LULC map	Climate data set	LULC map	
1	1970s	1973	1970s	1973	1970s	1973	Base period
2	1980s	1985	1970s	1985	1980s	1973	altered period1
3	1990s	1995	1970s	1995	1990s	1973	altered period2
4	2000s	2010	1970s	2010	2000s	1973	altered period3

Table 3: MK and Pettitt test for the rainfall and streamflow of UBNRB after TFPW at different time scale

Time scale	Stream flow					Rainfall				
	p-value		Sen's slope:	Change point	Pettit test	p-value		Sen's slope	Change point	Pettit test
	After*	Before*				After*	Before*			
Daily	< 0.0001	< 0.0001	0.013	1987	Increasing	0.387	0.953	0.000	1988	Increasing
Monthly	< 0.0001	0.031	0.378		No change	0.010	0.640	0.009		No change
annually	< 0.0001	0.009	9.619	1995	Increasing	0.006	0.260	1.886		No change
Kiremit	< 0.0001	0.014	20.30		No change	0.010	0.348	1.364		No change
Belg	< 0.0001	0.004	3.593	1985	Increasing	0.822	0.935	0.068		No change
Bega	0.000	0.214	4.832		No change	0.527	0.755	0.169		No change

* before and after TFPW, p: probability at 5% significance level

Table 4: Summary of precipitation indices of the UBNRB at decadal time series

Indices	1970s	1980s	1990s	2000s
Mean (mm)	4.17	4.05	4.42	4.16
95 percentile (mm)	12.57	12.52	13.66	13.31
99 percentile (mm)	17.34	17.77	19.44	19.65
1-day max (mm)	27.15	25.67	32.24	32.38
R20mm (days)	16	15	30	35
SDII (mm/day)	7.22	7.38	7.66	7.77

SDII is the ratio of total precipitation (mm) to R1mm (days).

Table 5: Confusion (error) matrix for the 2010 land use/cover classification map

LULC class	Water	Forest	Cultivated	Bushes and Shrubs	Row total	Producers' accuracy
Water	44	0	0	0	44	100
Forest	1	46	6	8	61	75.4
Cultivated land	2	3	77	15	97	79.4
Bushes and shrubs	1	3	9	73	86	84.9
Column total	48	52	92	86	288	
User's accuracy (%)	91.7	88.5	83.7	84.9		
Over all accuracy(%)	0.8					
Kappa	0.77					

Table 6: Statistical performance measure values of the SWAT model

Period		R^2	NSE	RVE (%)
	Calibration (1973-1977)	0.79	0.74	-3.41
1970s	Validation (1978-1980)	0.84	0.83	7.18
	Calibration (1983-1987)	0.80	0.74	-0.72
1980s	Validation (1988-19909	0.86	0.82	0.73
	Calibration (1993-1997)	0.91	0.91	1.79
1990s	Validation (1998-2000)	0.87	0.84	-3.56
	Calibration (2003-2007)	0.86	0.86	3.99
2000s	Validation (2008-2010)	0.94	0.92	-7.51

Table 7: SWAT sensitive model parameters and their (final) calibrated values for the four model runs.

Parameter	Optimum value			
	1970s	1980s	1990s	2000s
R-CN2	0.88	0.91	0.92	0.9
a-Alpha-BF	0.028	0.028	0.028	0.028
V-GW_REVAPMN	0.7	0.45	0.7	0.34
V-GWQMN	750	750	750	750
V-REVAPMN	550	450	425	550
a-ESCO	-0.85	-0.85	-0.85	-0.85
R-SOL_AWC	6.5	6.5	6.5	6.5

R: value from the SWAT database is multiplied by a given value, V: Replace the initial parameter by the given value, a: Adding the given value to initial parameter value.

Table 8: Water balance components analysis in the Upper Blue Nile River Basin (mm/year) by considering LULC and climate change over respective periods. All streamflow estimates are for El Diem station.

Water balance components	1970s	1980s	1990s	2000s
Surface flow (Qs)	112.8	143.4	168.6	141.4
Lateral flow (Ql)	116.8	113.35	125.9	117.6
Base flow (Qb)	47.3	29.6	9.8	64.7
PET (mm)	1615.1	1627.3	1614.7	1732.9
Ea (mm)	871.6	852.6	904.3	885
Precipitation (P)	1428.1	1397.1	1522.2	1462.5
Total yield (Qt)	276.9	286.3	304.3	323.7
Qs/Qt (%)	40.7	50.1	55.4	43.7
Qb/Qt (%)	17.1	10.3	3.2	20.0
Ea/P (%)	61.0	61.0	59.4	60.5
Qt/P (%)	19.4	20.5	20.0	22.1
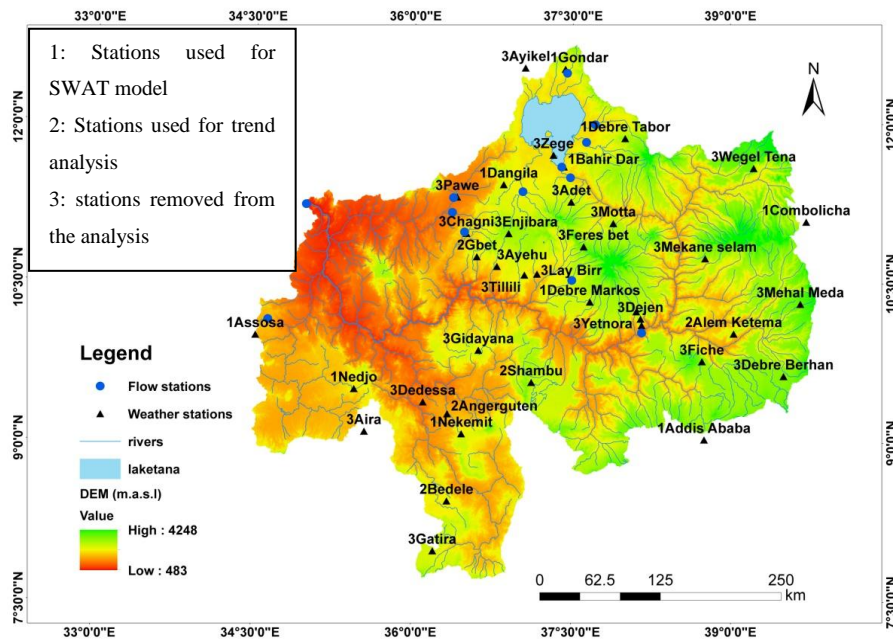
Figure 1 : Locations of study area and meteorological and discharge stations, with the Digital Elevation Model (DEM) data as the background
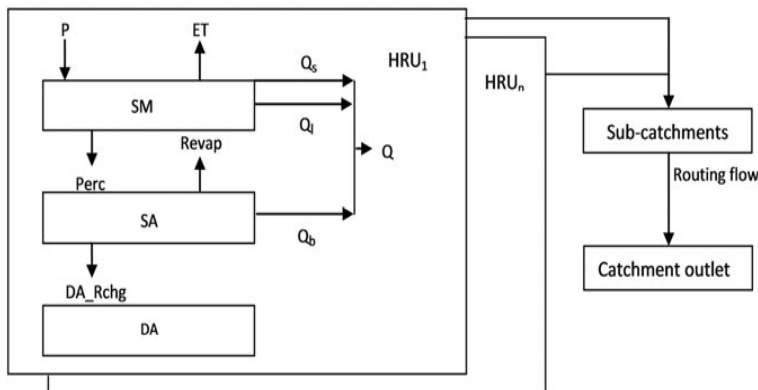
Figure 2: Schematic representation of the SWAT model structure from (Marhaento *et al.*, 2017)
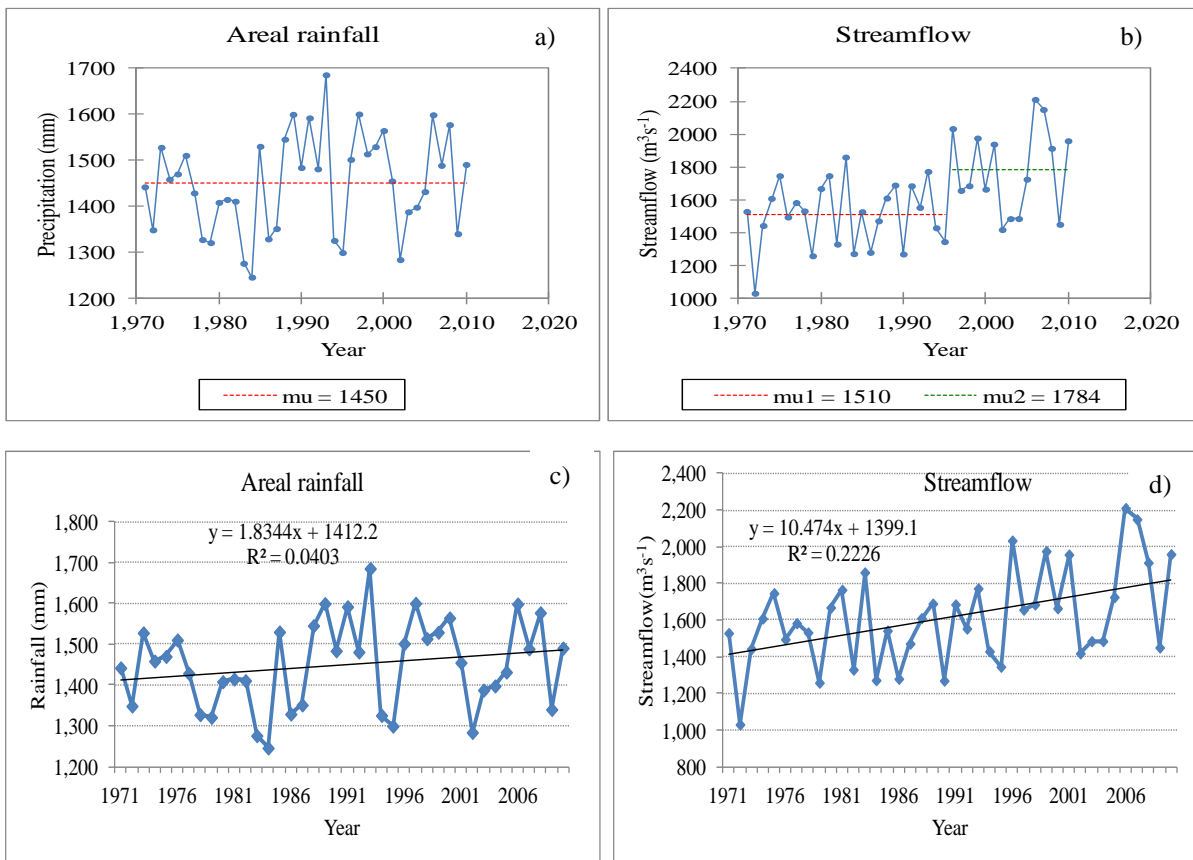
Figure 3: The Pettitt homogeneity test a) annual rainfall, b) annual flow of the UBNRB, C) linear trend of mean annual rainfall and d) linear trend of mean annual streamflow.

b)
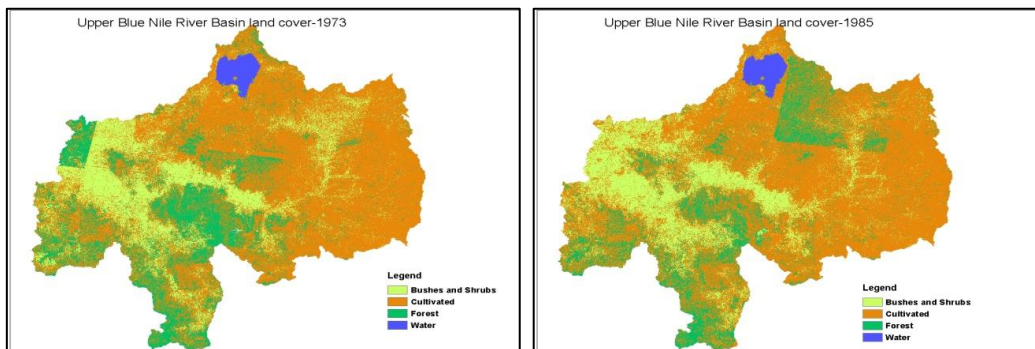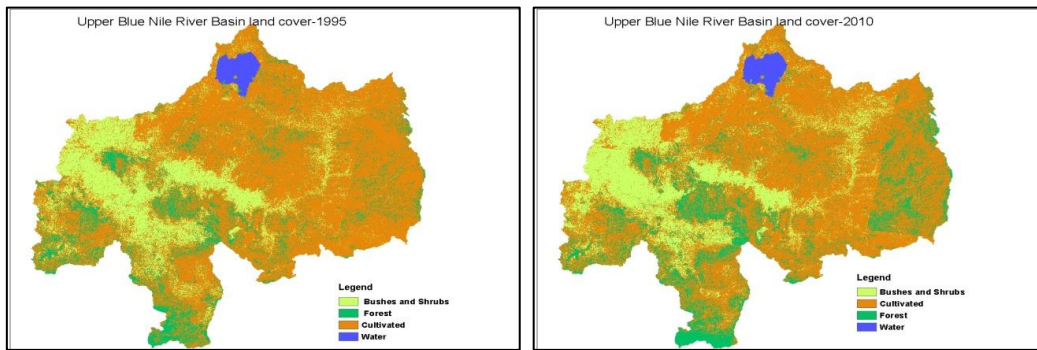
Figure 4: Landcover map of UBNRB derived from Landsat images a) 1973, b) 1985, c) 1995 and d) 2010

a)   b)
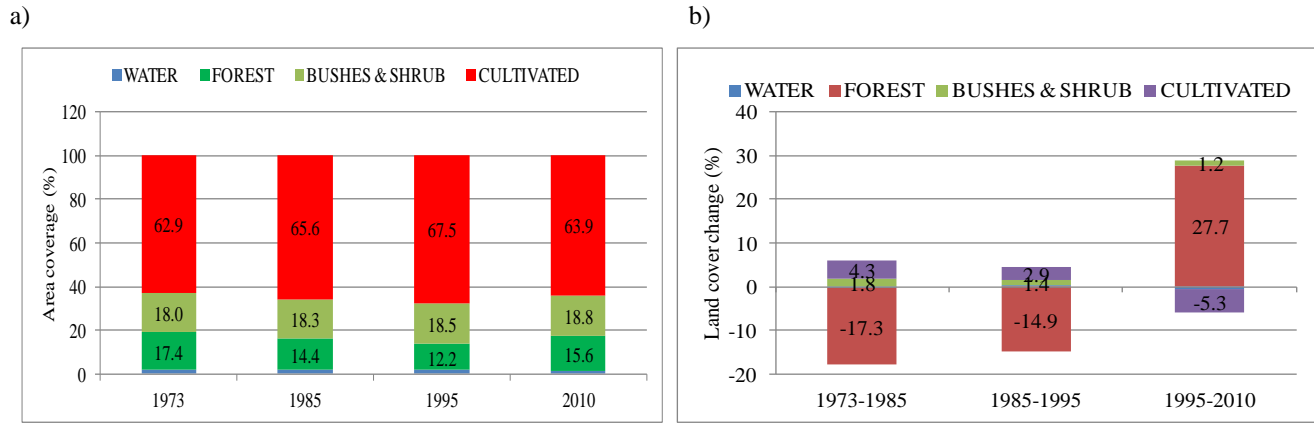
5   Figure 5: a) LULC composition, b) LULC change in the UBNRB during the period from 1973 to 2010

a)

b)

c)

d)
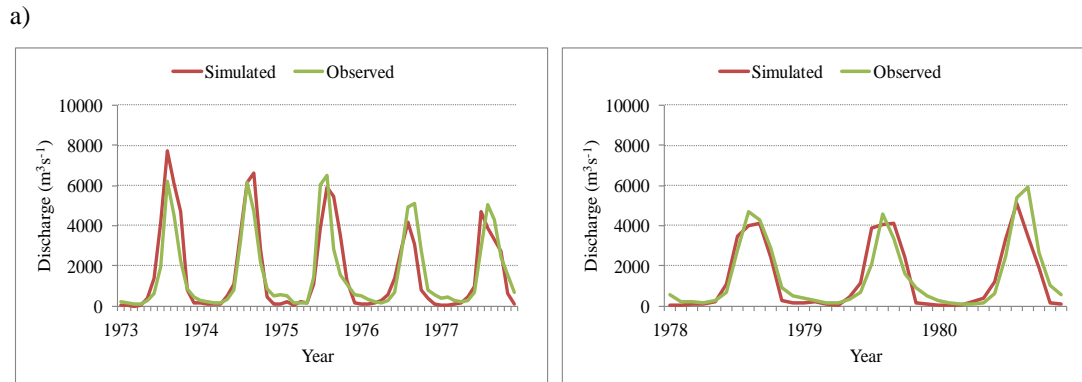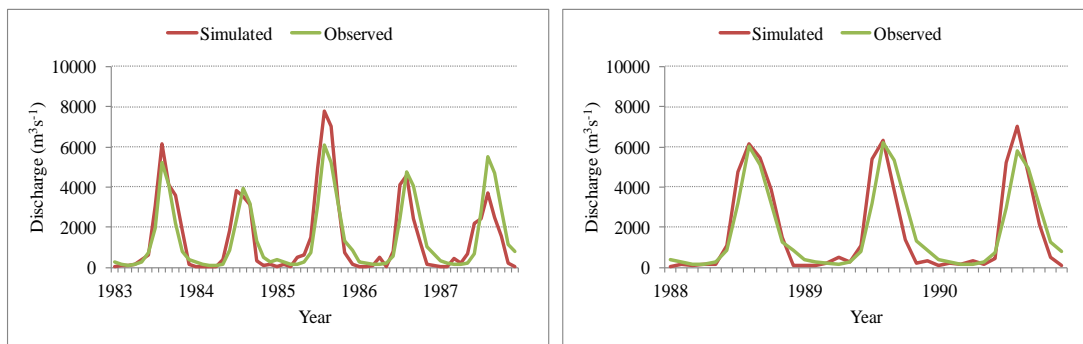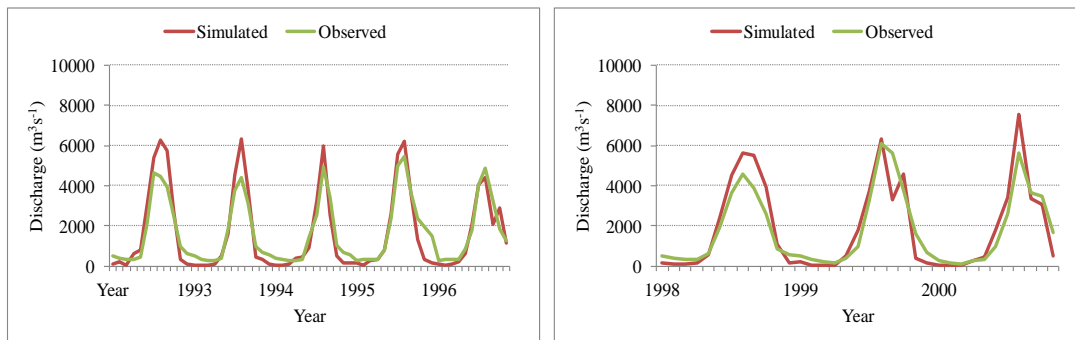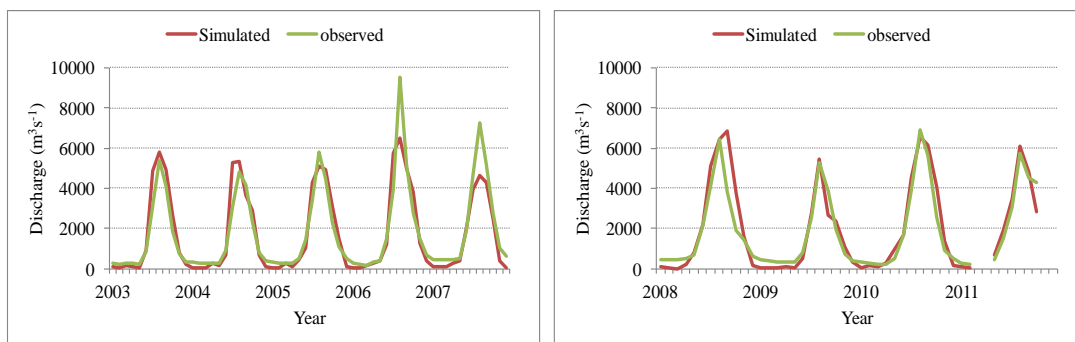
Figure 6: Calibration and validation of the SWAT hydrological model (left and right) respectively a) 1970s, b) 1980s, c) 1990s and d) 2000s monthly time scale
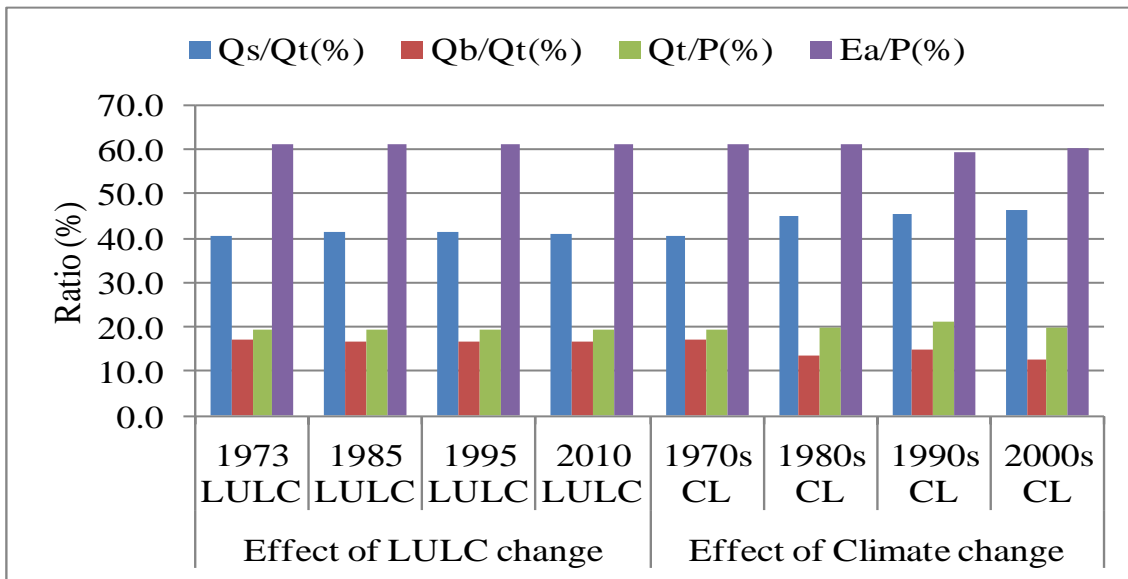
Figure 7: Ratio of water balance component analysis at El Diem station using a single effect (LULC/climate change).